August 1984

INT 116/84

NUMERICAL SIMULATIONS OF THE ELECTRON GUN

T.M. Tran

Centre de Recherches en Physique des Plasmas
Association Euratom - Confédération Suisse
Ecole Polytechnique Fédérale de Lausanne

1. General Considerations

In this chapter, some simple relations which are helpful for the electron gun design, are presented. The near-cathode region is represented in Fig. 1 along with its fundamental parameters. A number of additional parameters can also be defined or estimated by simple adiabatic theory. The current density, j_K, on the emitter strip is given by:

$$j_K = \frac{I}{2\pi R_K \ell_K} \tag{1}$$

The value of j_K must not exceed the space charge limited current density j_{sp} which is related to the potential drop at the cathode V_e by:

$$j_{sp} = .074\ V_e^{3/2}\ d_K^{-2} \qquad [A\,cm^{-2}] \tag{2}$$

where V_e is in kV and d_K in cm.

Assuming that the emitted electrons have their total velocities initially equal to zero, their oscillatory velocities are given by [1]:

$$V_{\perp K} = \frac{V_e}{d_K B_K} \tag{3}$$

Neglecting space charge effects and assuming adiabatic flow, the oscillatory velocity at the output of the gun (entrance of the energy extraction region) $v_{\perp 0}$ is related to $v_{\perp K}$ by:

$$\gamma_0 v_{\perp 0} = \left(\frac{B_0}{B_K}\right)^{3/2} \frac{V_e}{d_K B_0} \tag{4}$$

where γ_0 is the relativistic factor of the electrons given by:

$$\gamma_0 = 1 + \frac{V_e}{511} \tag{5}$$

V_a being the beam voltage in kV.
Since the longitudinal velocity v_{z0} is related to $v_{\perp 0}$ by:

$$v_{z0} = \left(\frac{2e}{m_e} V_a - v_{\perp 0}^2 \right)^{1/2} \tag{6}$$

we can see from Eq.(4), that for a given cathode geometry and magnetic field configuration, the maximum value of V_e is limited by:

$$V_e < B_k^{3/2} \frac{d_k}{\gamma_0} \left(\frac{2eV_a}{m_e B_0} \right)^{1/2} \tag{7}$$

For values of V_e higher than this limit, electrons will be reflected towards the cathode by the high magnetic field. It is interesting to note that higher magnetic field at the cathode will increase this limit on the control electrode potential V_e. Nevertheless, arcing considerations (E_k < 100 kV/cm) and sufficient clearance for the beam between the emitter and the control electrode impose other constraints.

Another helpful relation for the electrode gun design is obtained by invoking the angular momentum conservation (or Busch theorem):

$$R_k = \sqrt{\frac{B_0}{B_k}} R_0 \tag{8}$$

which relates the beam radius R_0 and the magnetic field B_0 at the gun output to the emitter radius R_K and the magnetic field B_k. This relation remains valid even when space charge is present.

All the precedent considerations, although useful, are not sufficient for an accurate optimization of the electron gun, since the space charge effects are neglected. Moreover, the spread in electron velocities (which is an important parameter for the gyrotron) cannot be calculated. In the next two sections, numerical simulations of the electron trajectories are discussed. In most of the calculations presented in the following, the gun parameters d_k, ℓ_k, R_k and ϕ are fixed and given in Tab. 1.

d_K	4 mm
ℓ_K	3 mm
R_K	9 mm
ϕ	30 °

Tab. 1 Cathode parameters

2. Numerical model

The Herrmannsfeldt EGUN code [2] is used to simulate the electron trajectories in the electron gun. The effects of space charge and self magnetic fields as well as the realistic geometry of the gun are accounted for. The magnetostatic field required to adiabatically compress the beam is computed by a magnetic field code which calculates the B-fields from a given axisymmetrical coil structure [3]. The output from this magnetic code consists of a table of the azimuthal components A_Θ of the vector potential, defined on a 2-D (r,z) mesh. From this table, EGUN computed the required B_Z and B_r fields by numerical interpolation and differentiation. The relevant characteristics of the beam at the entrance of the energy extraction region are determined by the averaged values and standard deviation of the electron velocities defined by:

$$\bar{v}_{\perp(z)} = \frac{1}{N} \sum_{j=1}^{N} v_{\perp(z)_j} \qquad (9.a)$$

$$\Delta v_\perp = \left[\frac{1}{N} \sum_{j=1}^{N} \left(v_{\perp j} - \bar{v}_\perp \right)^2 \right] \qquad (9.b)$$

$$\alpha = \bar{v}_\perp / \bar{v}_z \qquad (9.c)$$

The total number of trajectories N is taken as high as 48 in most of our calculations. The mesh interval (in both directions r and z) is equal to 0.25 mm in computing trajectories between the cathode to the

cavity region. This high spatial resolution is required to describe accurately space charge effects which dominate near the emitter region. From the cavity region to the collector, the mesh interval is taken larger since space charge effects are no more important and the electron beam widen. Interactions between the electrons and the A.C. cavity fields are not accounted for in this model.

3. Numerical results

Two types of problems are treated there. The first type is the sensitivity of the beam performance at the entrance of the energy extraction region, to the variations of the gun parameters and the static magnetic field shape at the cathode. In the second problem, we try, with the same numerical code, to estimate the power density distribution on the electron collector.

3a. Beam performance

We have defined the beam performance essentially by the velocity ratio α and $\Delta v_\perp / v_\perp$ defined in Eqs. (9), at the entrance of the cavity region.

In a preliminary set of calculations, we have analyzed the sensitivity of α and $\Delta v / v$ for three guns respectivity labeled by GUN 7, GUN 8, and GUN 9. They differ only by the cathode shape (c.f. Figs 2a, 2b, 2c). All three guns are immersed in a static B-field produced by the coil system represented in Fig. 3. The anode potential V_a is 70 keV and the beam current, 10 A. By comparing the curves in Figs. 4, we can see that the velocity spread $\Delta v_\perp / v_\perp$ is much higher for the $\phi = 25^\circ$ gun than the other two. This is possibly due to the non-laminar flow near the emitter in the $\phi = 25^\circ$ gun (Fig. 2b). Changing the shape of the "cathode nose" (Gun 9, Fig. 2c) merely shift the performance curve. For values of V_e higher than those represented in Figs. 4, we found that electrons are reflected by the high B-field region, as predicted by the relation (7).

From this, we have decided to consider only the GUN 7 geometry in the investigation of the influence of the B-field shape on beam performances. Due to technological constraints, the coil structure is now slightly changed (Fig. 5). To simulate the variation of the B-field shape on the emitter strip, we have done calculations for different positions on the emitter center, keeping the coil positions fixed. Values of α and $\Delta v_\perp / v_\perp$ are given versus the derivative dB_z/dz defined on the center of the emitter, whose axial positions (in cm) appear as labels on Fig. 6. The values of the beam performance correspond to those found at 29.1 cm beyond the emitter cathode. From these calculations, it seems that the velocity spread is very sensitive to the static B-field shape on the cathode. To investigate in more details this effect, we have fixed the axial position of the emitter center at z_c=-22.8 cm. The current in each of the four coils shown in Fig. 5 is given by the following requirements.

- At the entrance of the energy extraction region (z=22.3 cm, r=.2 cm) the B_z-field is determined by the resonance condition for 120 GHz gyrotron :

$$B_z = 4.23 \frac{\Omega}{\omega} \quad [T] \tag{10}$$

and decreases linearly by 8% over 5.6 cm. In the following calculations, Ω/ω=1.13.

- On the emitter (z=-22.8 cm, r=.9 cm), the B-field is deduced from Eq. 8, since all the others parameters are fixed. The last condition, which is necessary for the determination of the current, is the slope of the axial field dB_z/dz.

The influence of this slope on the beam performance at z=16.3 cm (where B_z=5.22 T) is shown in Fig. 7. From these curves, it seems that the velocity spread is less sensitive to the slope variations, than the previous calculations. This can be expected if we note that the emitter position (z=-22.8 cm) relative to the coils, is already optimized (c.f. Fig. 6).

The beam performance curves, versus the control electrode potential V_e, the anode potential V_a and the beam current I, are shown respectively in Figs. 8-10. It is interesting to note that space-charge-effects cannot be neglected, even for a beam current of 3 A and that they decrease strongly the perpendicular velocity for I>10 A.

The main conclusions of these extensive numerical computations may be summarized as follows :

- For a given coil structure, the axial position of the electron gun emitter and the current in the gun coils, are critical if a minimum velocity spread is required.

- A 10 A, 70 keV electron beam with $\alpha \simeq 1.5$ and $\Delta v_\perp / v_\perp \simeq 3\%$ can be produced by the electrode configuration of the proposed electron gun.

3b. The electron collector

We have performed some simulations of the electron trajectories from the emitter to the collector with the numerical code described in chap. 2 (Fig. 11). The interaction between electrons and the A.C. cavity fields is neglected in these simulations. This implies that the energy flux calculated on the collector would be rather pessimistic. On the other hand, the collector axial position determined by this method, could be inaccurate.

Fig. 12 shows the distribution of the heat flux on the collector when the static B-field is decreased to 0. T at z=3.5 m, by two coils placed in the collector region [3]. Increasing this collector field from 0 to 10 G does not change very much this heat flux distribution. Since about 30% of the electron beam power is lost in the resonator, a value of 500 W/cm^2 for the peak heat flux on the collector seems quite realistic.

Trajectory calculations with appropriate electron distribution at the output of the energy extraction region (determined by a cavity-beam interaction code) will be done in order to estimate more accurately the axial position of the electron collector.

REFERENCES

[1] Gol'denberg A.L., Petelin M.I., Radiophys. Quant. Electronics, 15 (1973), 106

[2] Herrmannsfeldt W.B., SLAC-Report-226, Stanford Linear Accelerator Center, Standfort, California (1979)

[3] Tran M.Q.

FIGURE CAPTIONS

Fig. 1 The near-cathode region.

Fig. 2a Electron flow near the emitter in GUN#7.

Fig. 2b Electron flow near the emitter in GUN#8.

Fig. 2c Electron flow near the emitter in GUN#9.

Fig. 3 Stucture of coils.

Fig. 4a Velocity ratio α and velocity spread $\Delta v_\perp / v_\perp$ versus control electrode potential V_e for the $\phi=30^\circ$ guns.

Fig. 4b Velocity ratio α and velocity spread $\Delta v_\perp / v_\perp$ versus control electrode potential V_e for the $\phi=25^\circ$ gun.

Fig. 5 Disposition of coils and the B_z-profile on the axis.

Fig. 6 Variations of the velocity ratio α and the velocity spread $\Delta v_\perp / v_\perp$ versus z-derivative of B_z defined on the electron emitter. Each point of the curve is labelled by the axial position of the emitter in cm.

Fig. 7 Variations of the velocity ratio α and the velocity spread $\Delta v_\perp / v_\perp$ versus z-derivative of B_z defined on the electron emitter. The axial position of the emitter is fixed.

Fig. 8 Variations of the velocity ratio α and the velocity spread $\Delta v_\perp / v_\perp$ versus the control electrode potential. The emitter is at z=-22.8 cm, the z-derivative of B_z on the emitter $dB_z/dz=30$ G/mm, the beam current I=10 A., the anode potential $V_a=70$ kV.

Fig. 9 Variations of α and $\Delta v_\perp / v_\perp$ versus V_a. The control electrode is at 30 kV, all the other parameters are the same as in Fig. 8.

Fig. 10 Variations of α and $\Delta v_\perp / v_\perp$ versus I. The parameters are the same as on Fig. 8 and Fig. 9.

Fig. 11 Electron trajectories from the electron gun emitter to the electron collector.

Fig. 12 Heat flux distribution on the collector for an electron energy flux of 700 kW. The collector radius is 15 cm.

FIG. 1

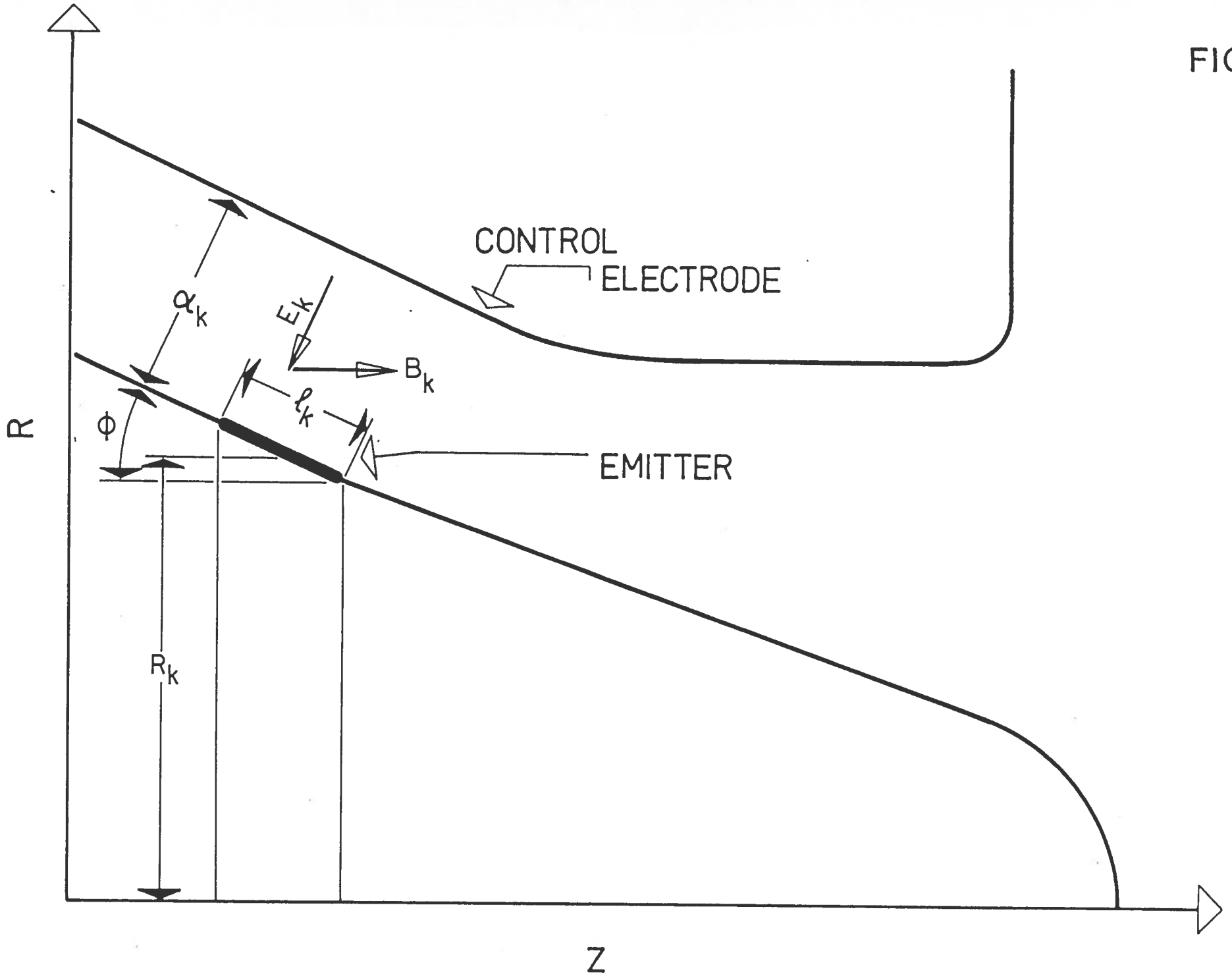

FIG.2a

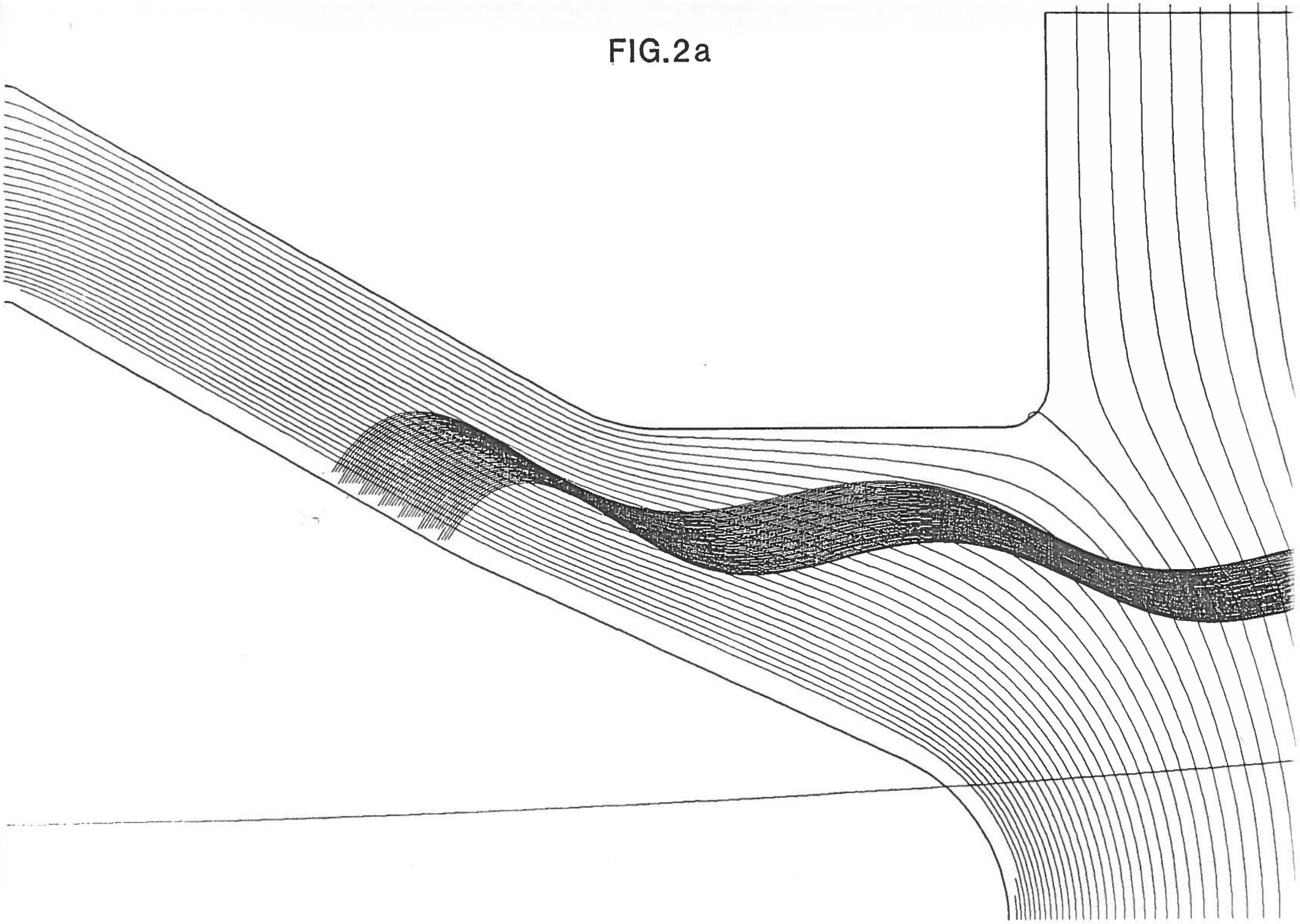

FIG. 2b

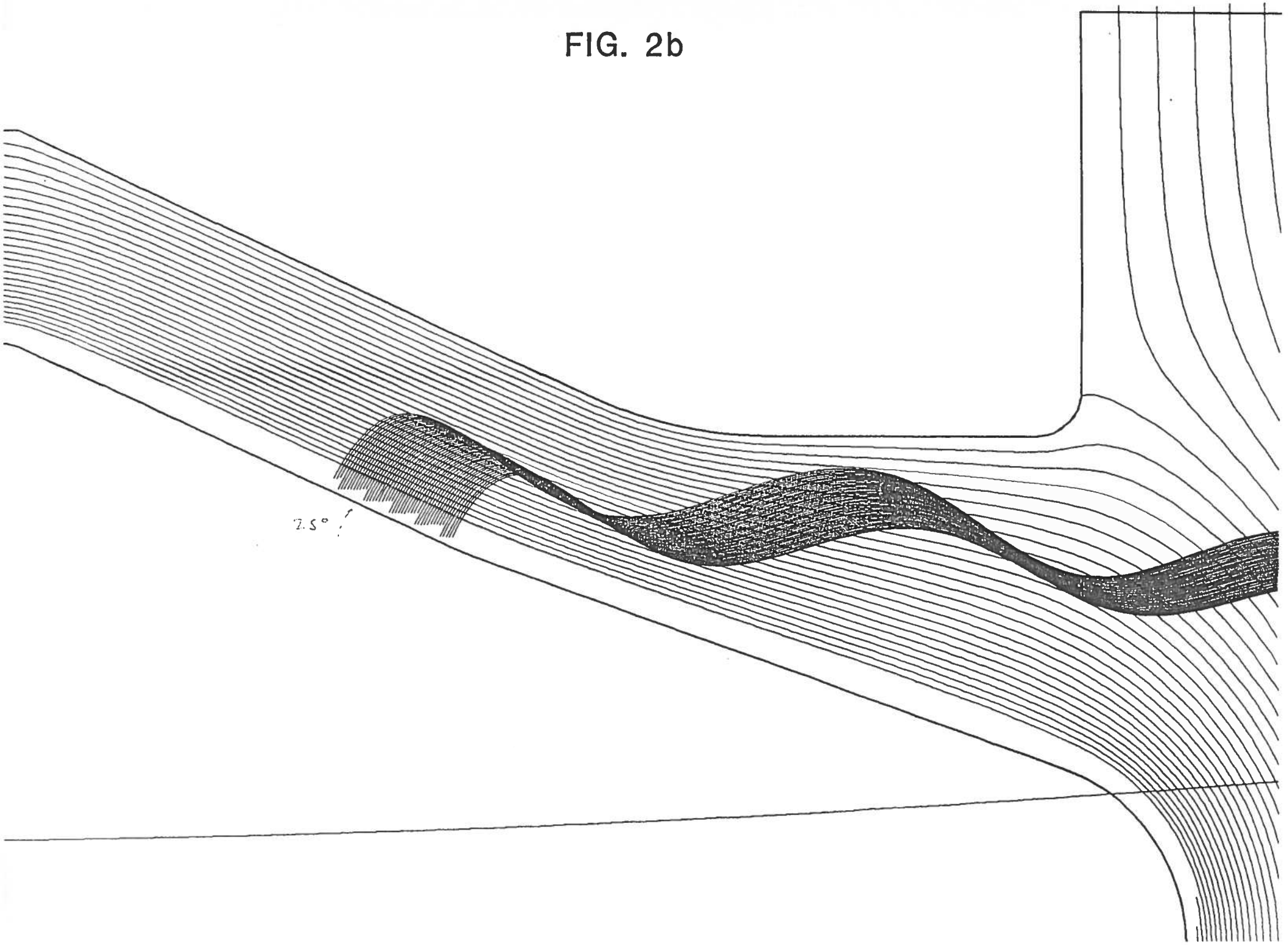

FIG. 2c

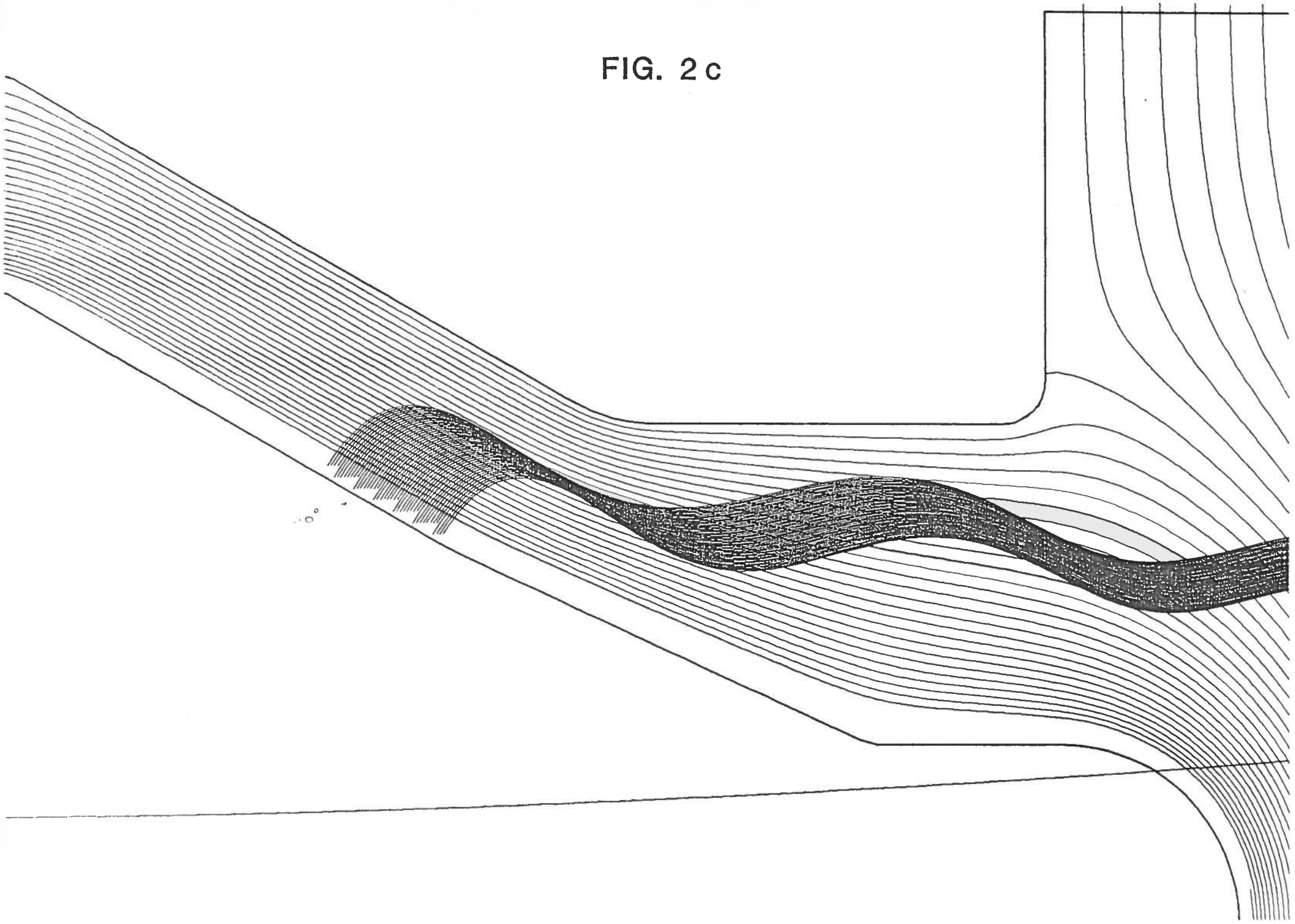

FIG. 3

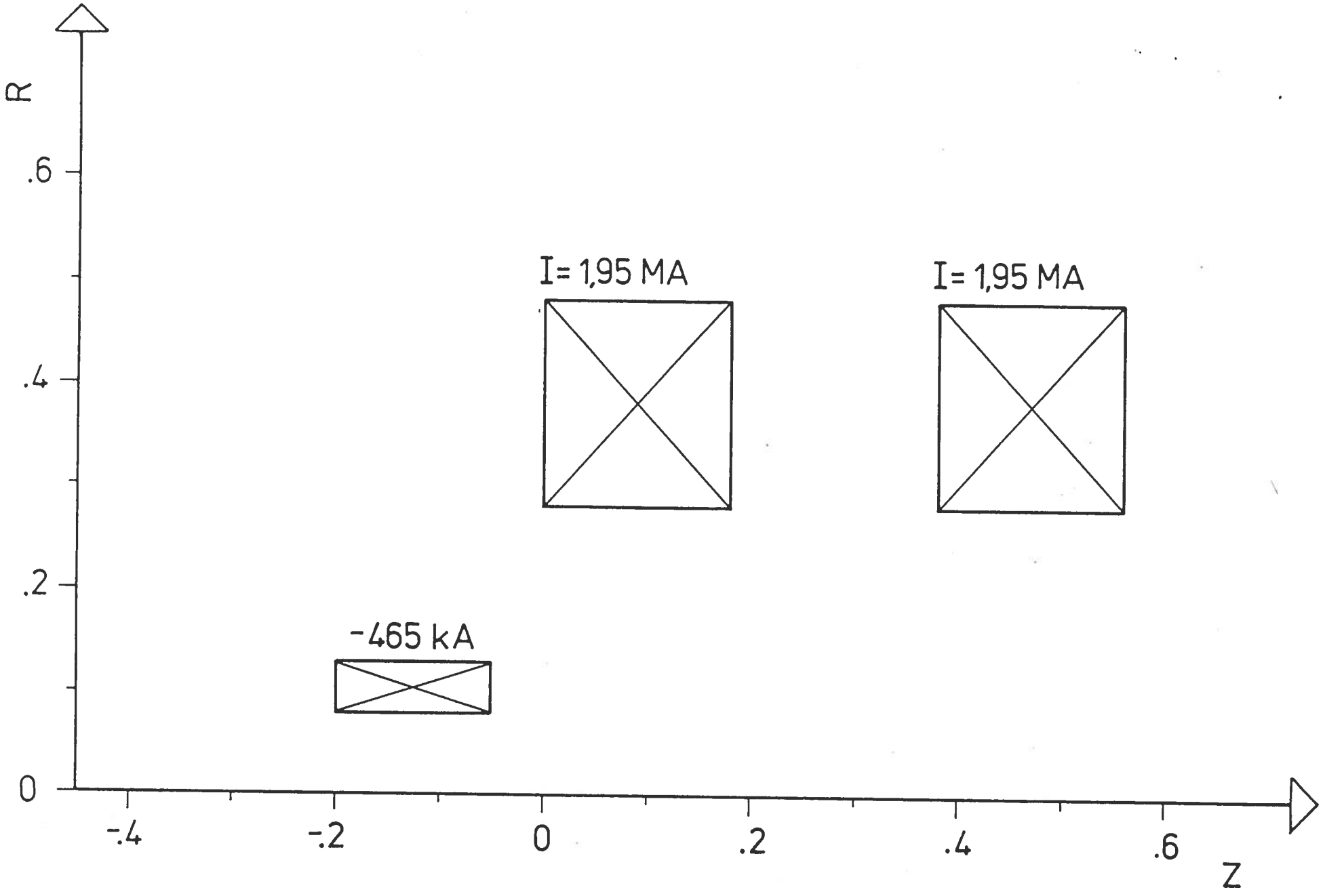

FIG. 4a

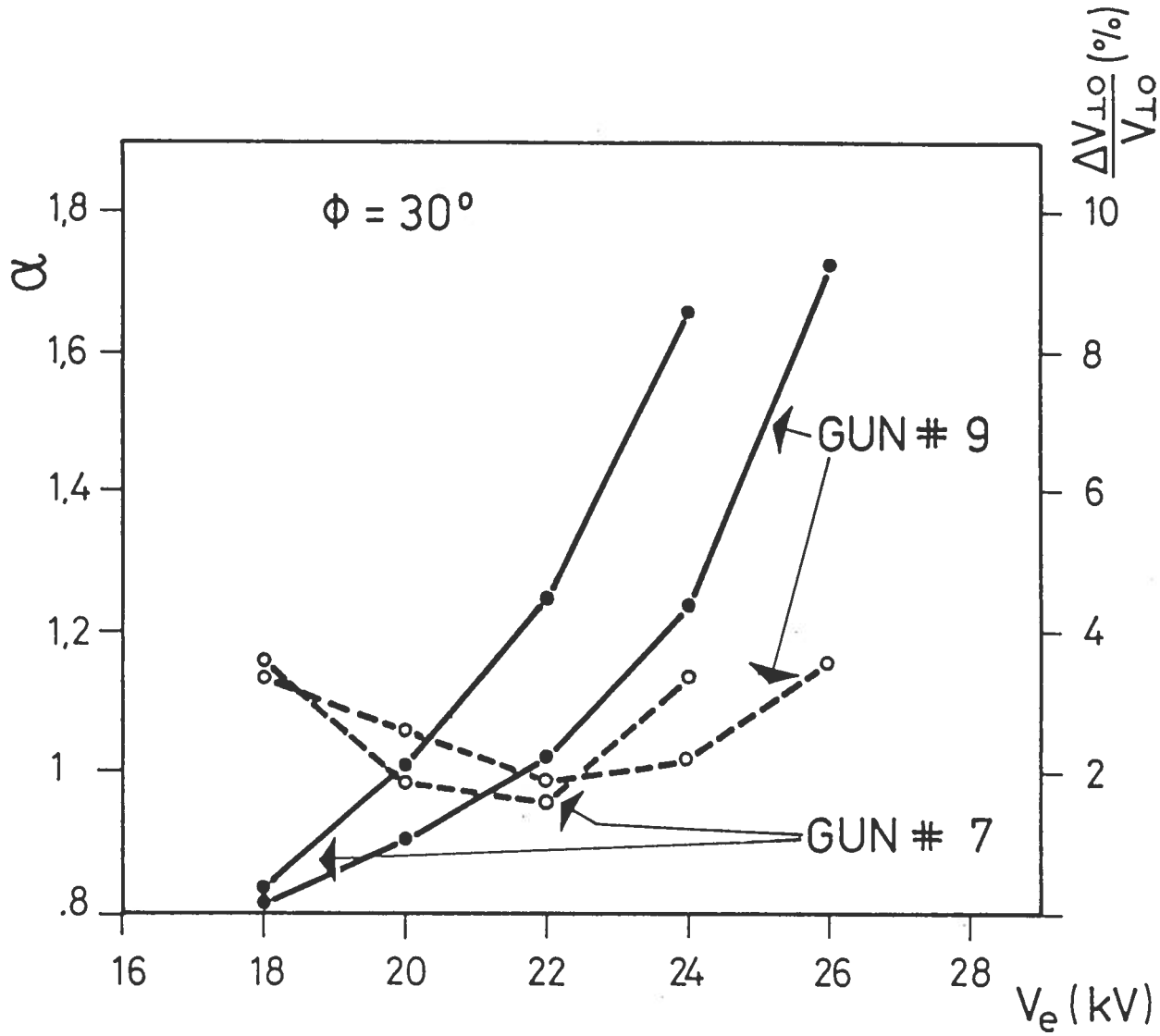
Φ = 30°
α
1,8
1,6
1,4
1,2
1
.8
16
18
20
22
24
26
28
V_e (kV)
$\frac{\Delta V_{\perp o}}{V_{\perp o}}$ (%)
10
8
6
4
2
GUN # 9
GUN # 7

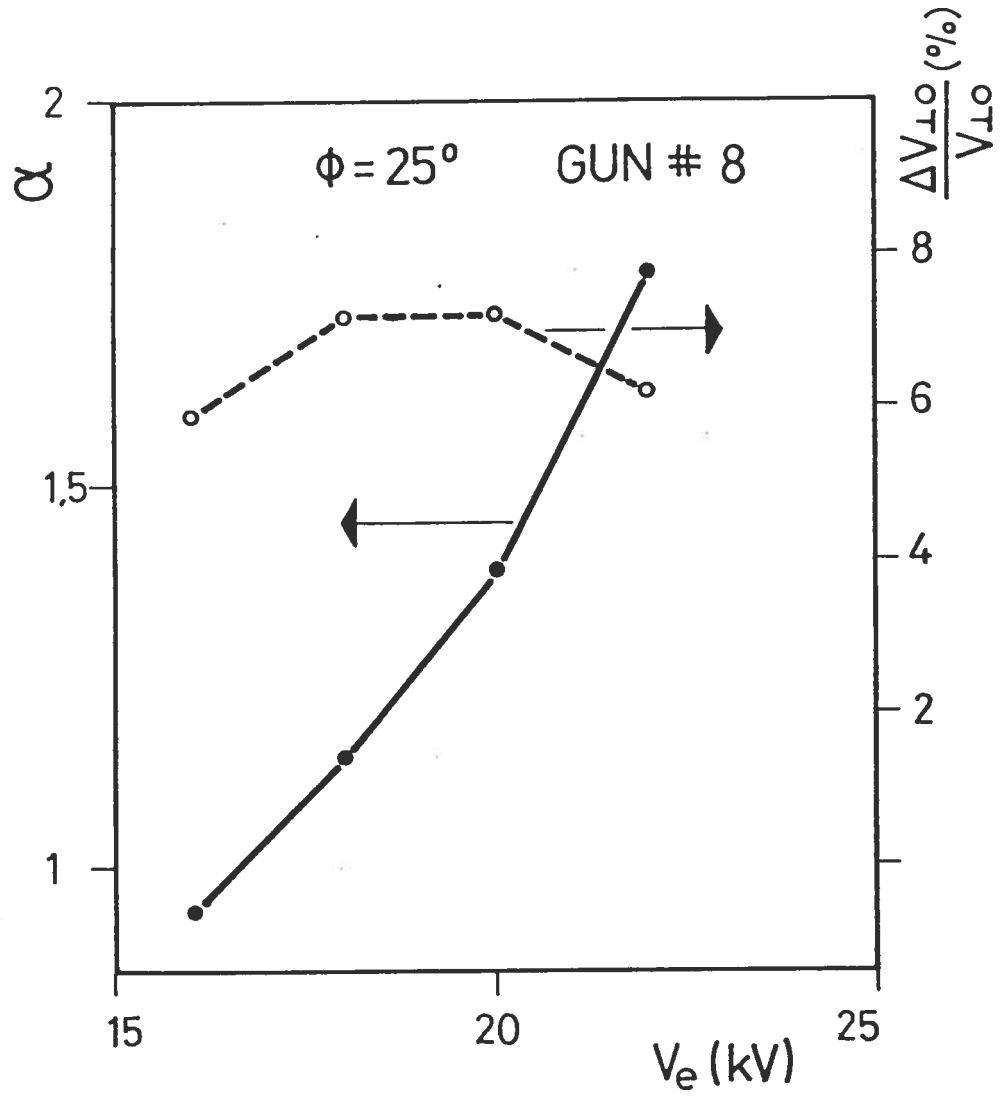

FIG. 4b

FIG. 5

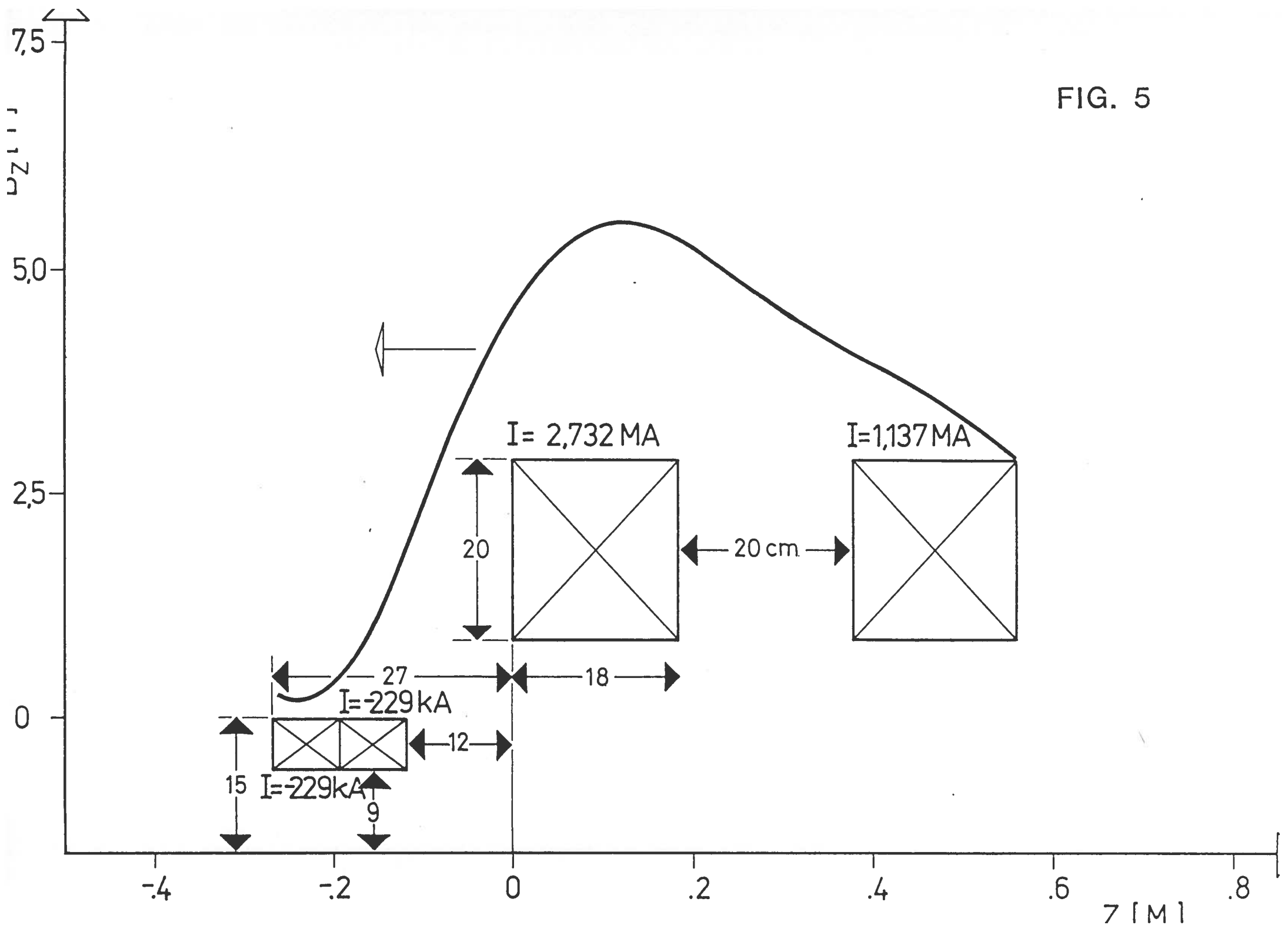
7,5
5,0
2,5
0
-.4
-.2
0
.2
.4
.6
.8
z [M]
I= 2,732 MA
I=1,137 MA
20
20 cm
27
18
I=-229 kA
12
15
I=-229kA
9

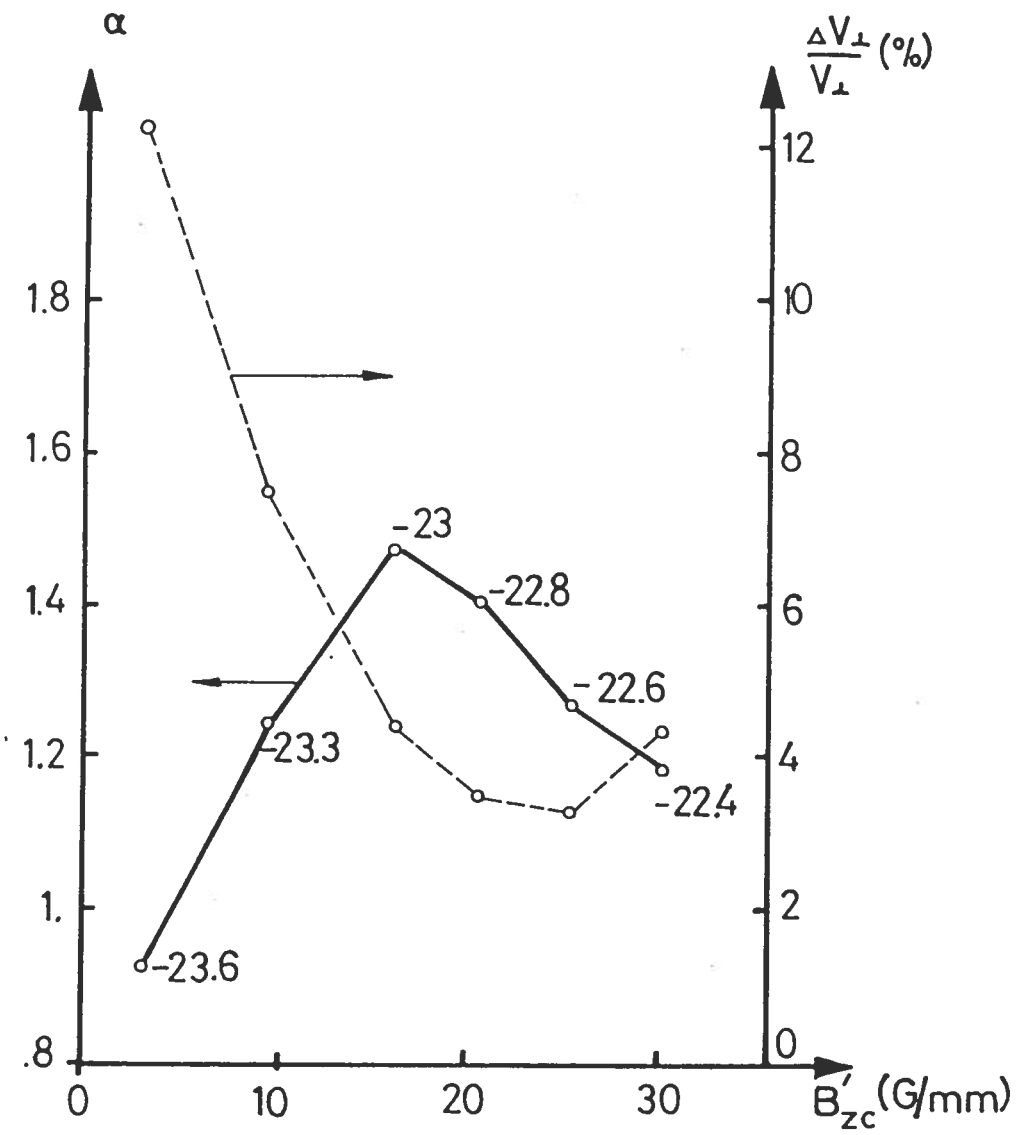
α
ΔV⊥/V⊥ (%)
1.8
1.6
1.4
1.2
1.
.8
12
10
8
6
4
2
0
-23
-22.8
-22.6
-22.4
-23.3
-23.6
0
10
20
30
B'zc (G/mm)

FIG. 6

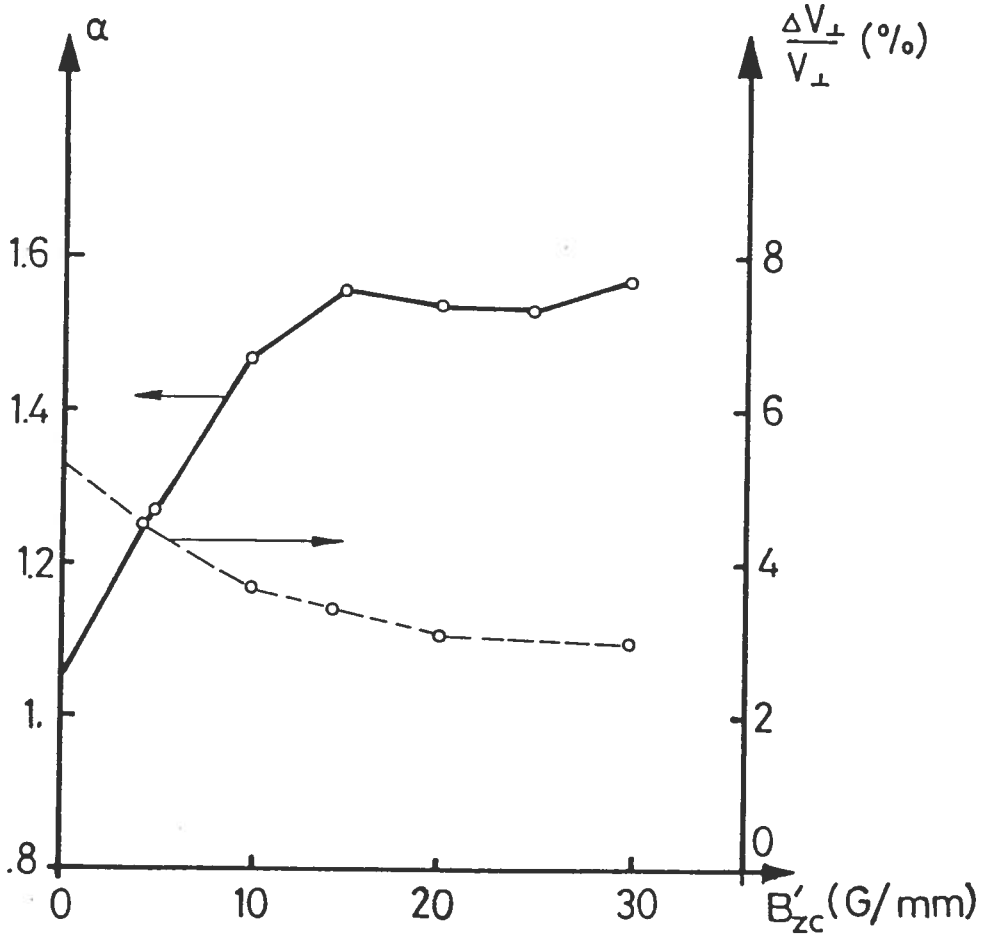

FIG. 7

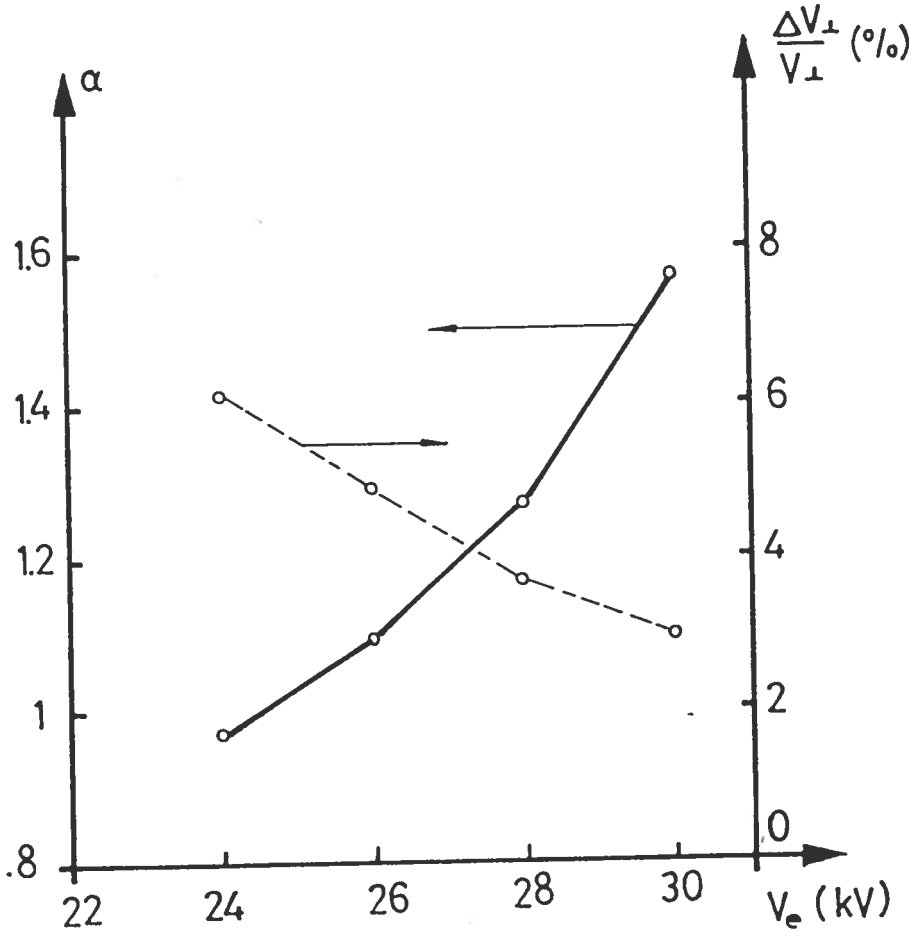

FIG. 8

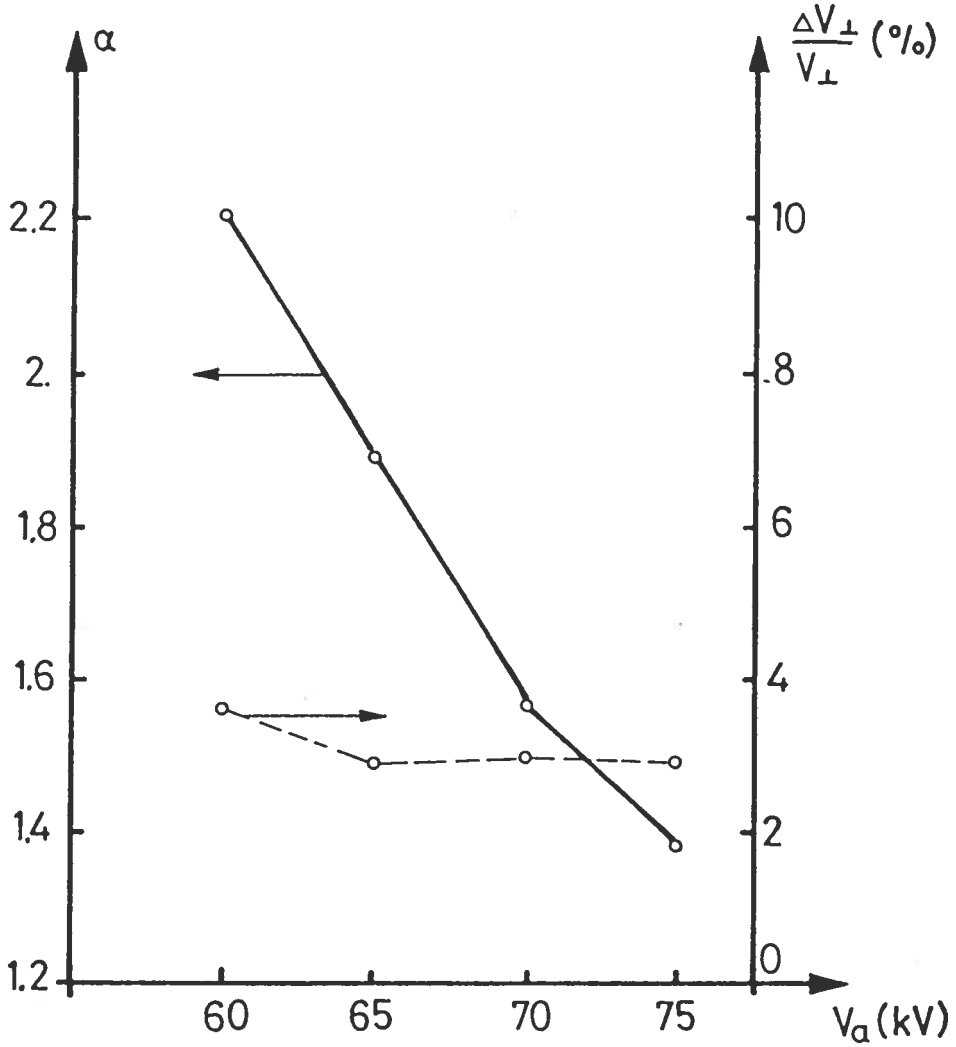

FIG. 9

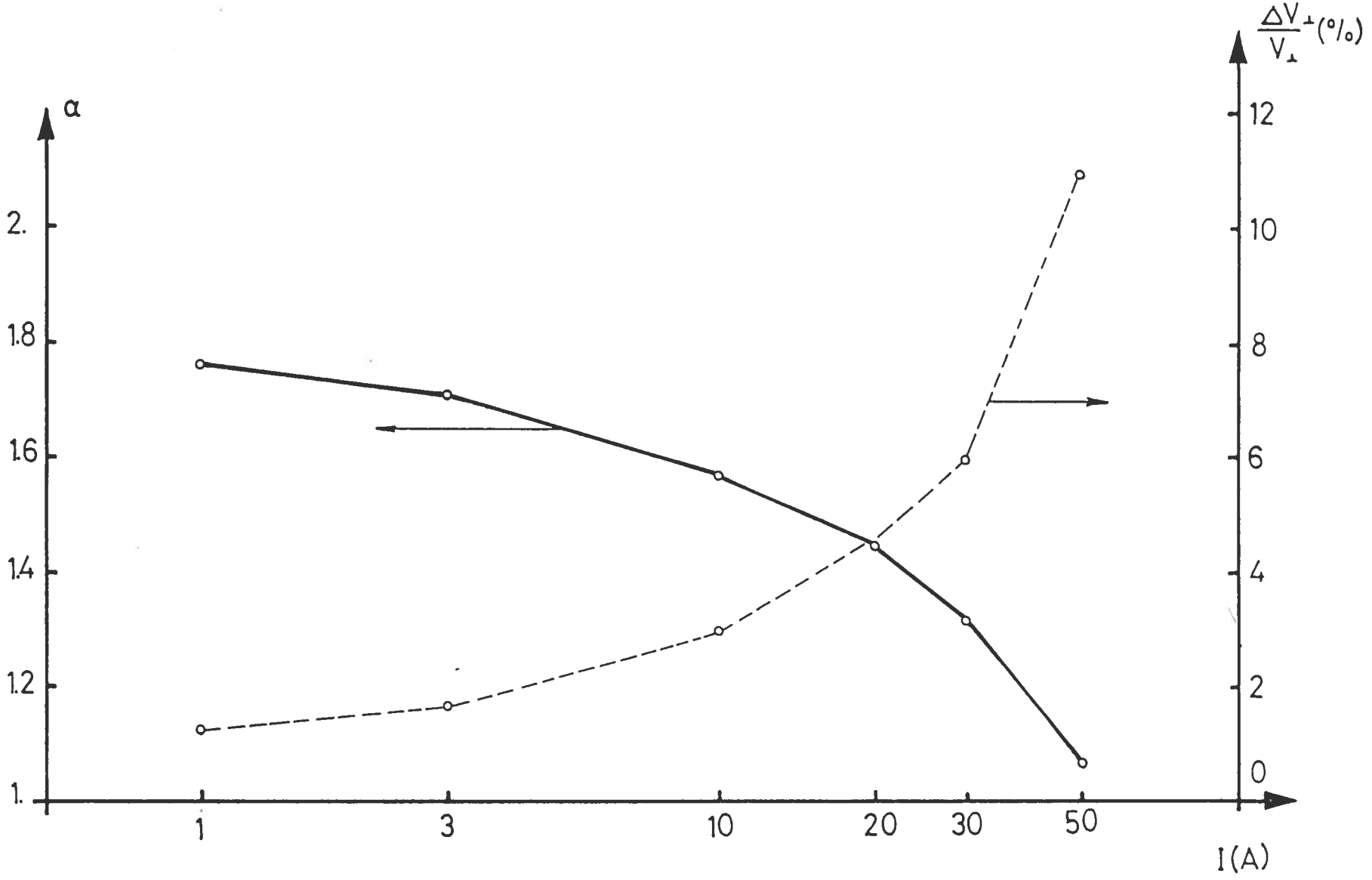

FIG. 10

FIG. 11

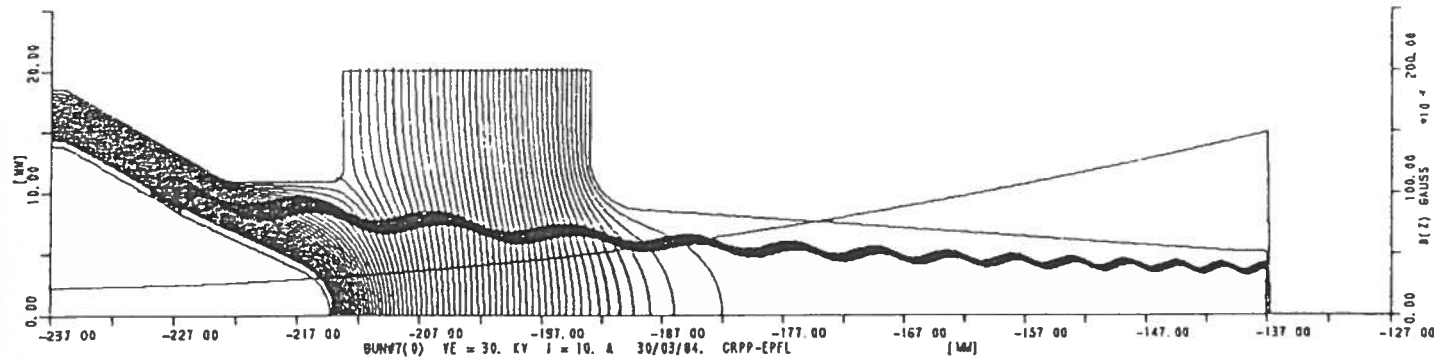
[MM]
20.00
10.00
0.00
-237.00
-227.00
-217.00
-207.00
-197.00
-187.00
-177.00
-167.00
-157.00
-147.00
-137.00
-127.00
B(Z) GAUSS
[MM]

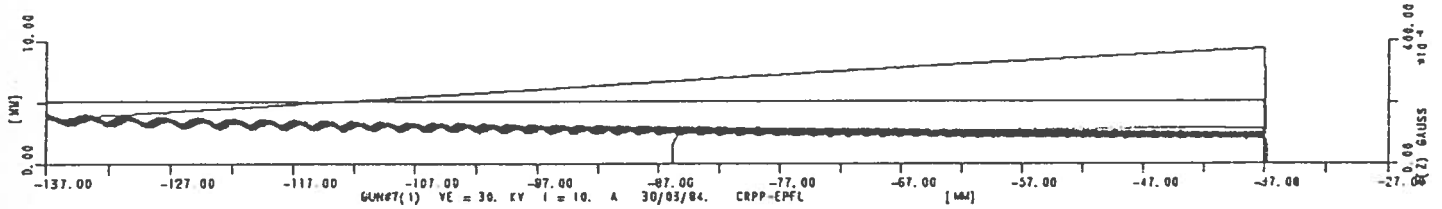
[MM]
10.00
0.00
-137.00
-127.00
-117.00
-107.00
-97.00
-87.00
-77.00
-67.00
-57.00
-47.00
-37.00
-27.00
B(Z) GAUSS
[MM]

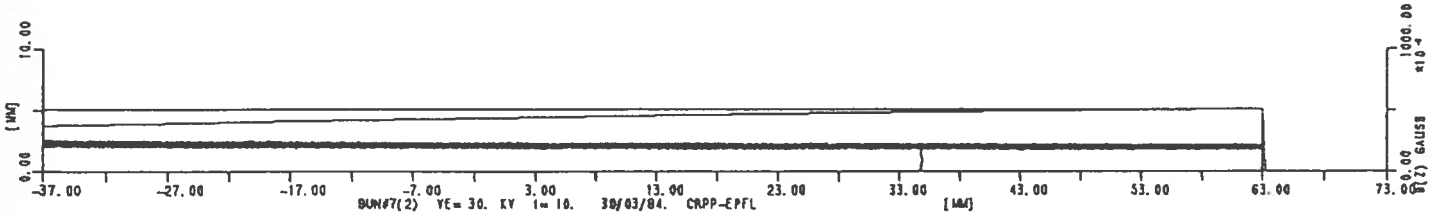
[MM]
10.00
0.00
-37.00
-27.00
-17.00
-7.00
3.00
13.00
23.00
33.00
43.00
53.00
63.00
73.00
B(Z) GAUSS
[MM]

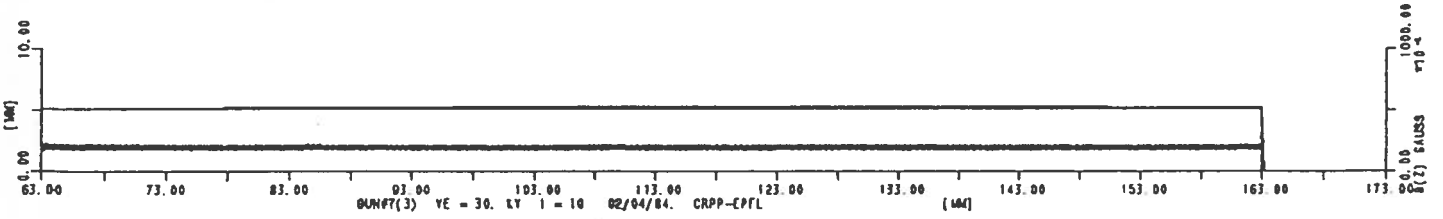
[MM]
10.00
0.00
63.00
73.00
83.00
93.00
103.00
113.00
123.00
133.00
143.00
153.00
163.00
173.00
B(Z) GAUSS
[MM]

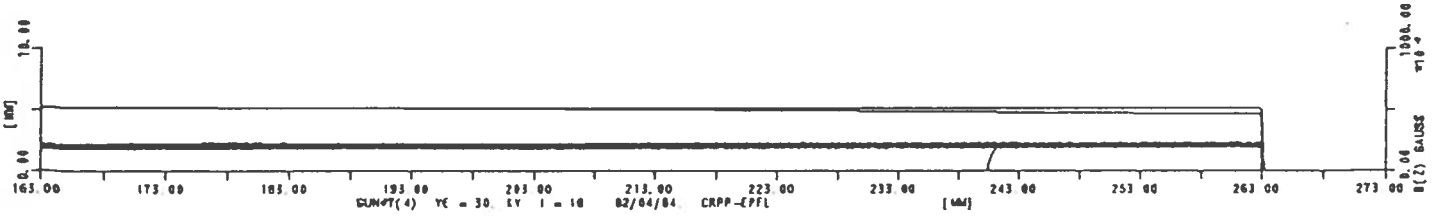
[MM]
10.00
0.00
163.00
173.00
183.00
193.00
203.00
213.00
223.00
233.00
243.00
253.00
263.00
273.00
B(Z) GAUSS
[MM]

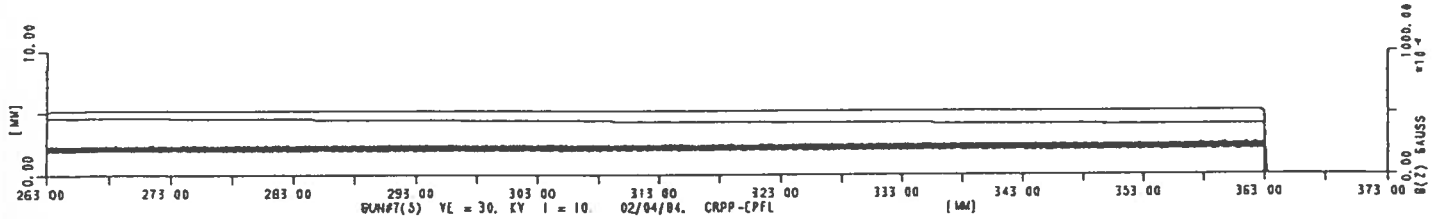
10.00
[MW]
0.00
263.00
273.00
283.00
293.00
303.00
313.00
323.00
333.00
343.00
353.00
363.00
373.00
[MM]
1000.00
*10-4
0.00
B(Z) GAUSS
GUN#7(5) VE = 30. KV I = 10. 02/04/84. CRPP-EPFL

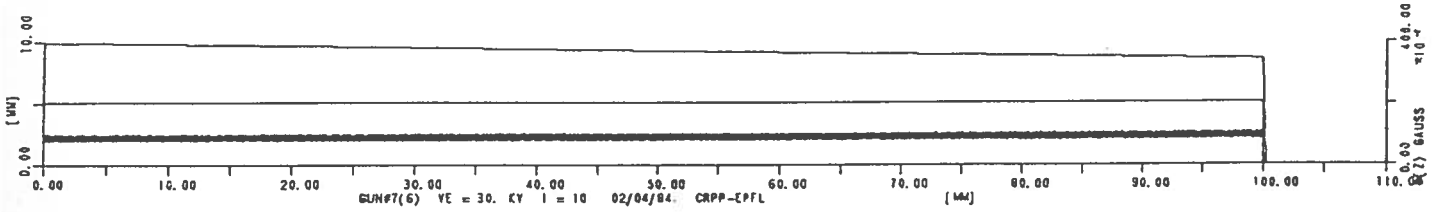
10.00
[MW]
0.00
0.00
10.00
20.00
30.00
40.00
50.00
60.00
70.00
80.00
90.00
100.00
110.00
[MM]
400.00
*10-4
0.00
B(Z) GAUSS
GUN#7(6) VE = 30. KV I = 10. 02/04/84. CRPP-EPFL

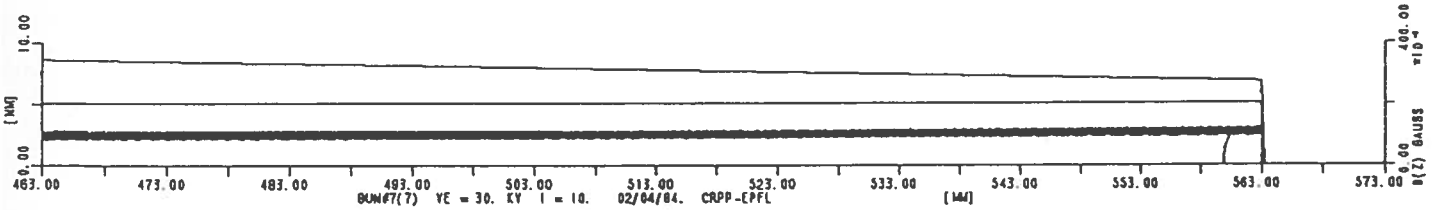
10.00
[MW]
0.00
463.00
473.00
483.00
493.00
503.00
513.00
523.00
533.00
543.00
553.00
563.00
573.00
[MM]
400.00
*10-4
0.00
B(Z) GAUSS
GUN#7(7) VE = 30. KV I = 10. 02/04/84. CRPP-EPFL

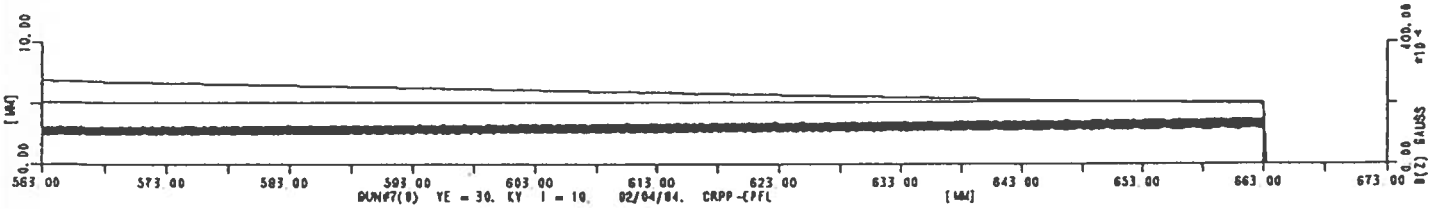
10.00
[MW]
0.00
563.00
573.00
583.00
593.00
603.00
613.00
623.00
633.00
643.00
653.00
663.00
673.00
[MM]
400.00
*10-4
0.00
B(Z) GAUSS
GUN#7(8) VE = 30. KV I = 10. 02/04/84. CRPP-EPFL

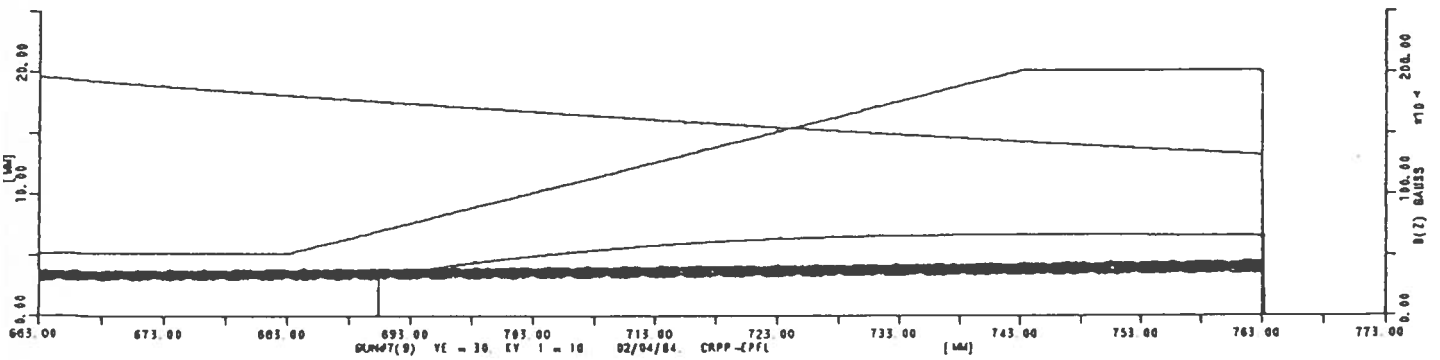
20.00
[MW]
10.00
0.00
663.00
673.00
683.00
693.00
703.00
713.00
723.00
733.00
743.00
753.00
763.00
773.00
[MM]
200.00
*10-4
100.00
0.00
B(Z) GAUSS
GUN#7(9) VE = 30. KV I = 10. 02/04/84. CRPP-EPFL

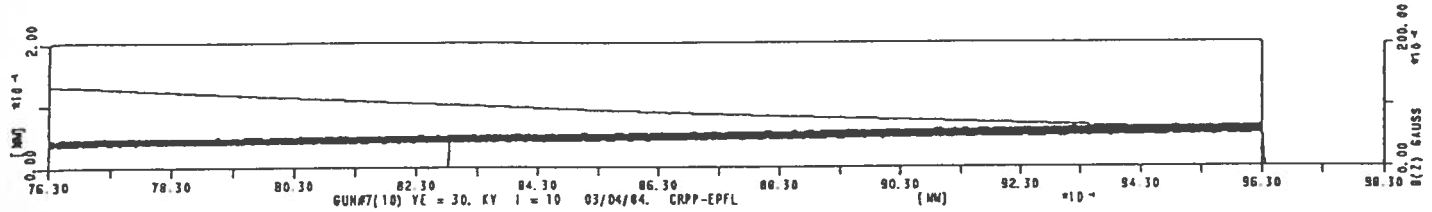
GUN#7(10) YE = 30. KY I = 10 03/04/84. CRPP-EPFL
[MM]
B(Z) GAUSS

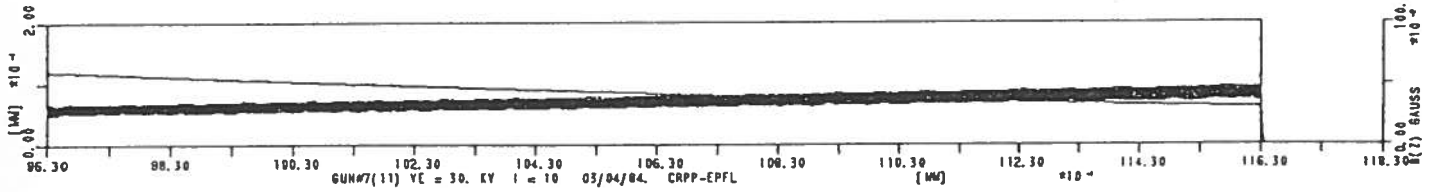
GUN#7(11) YE = 30. KY I = 10 03/04/84. CRPP-EPFL
[MM]
B(Z) GAUSS

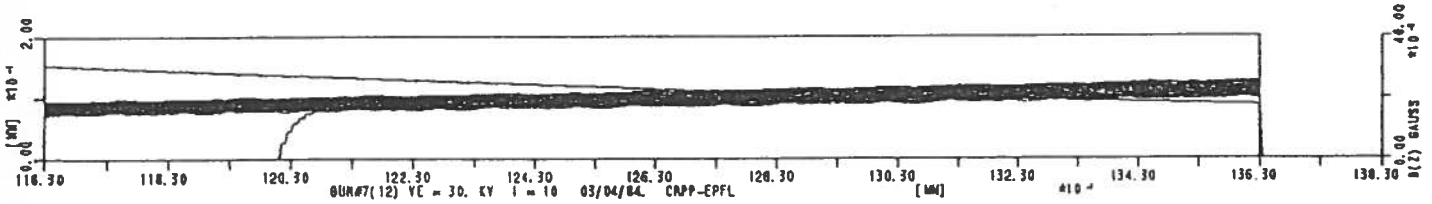
GUN#7(12) YE = 30. KY I = 10 03/04/84. CRPP-EPFL
[MM]
B(Z) GAUSS

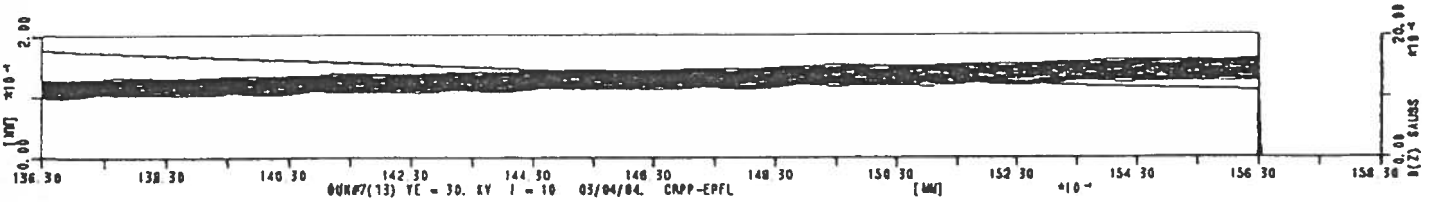
GUN#7(13) YE = 30. KY I = 10 03/04/84. CRPP-EPFL
[MM]
B(Z) GAUSS

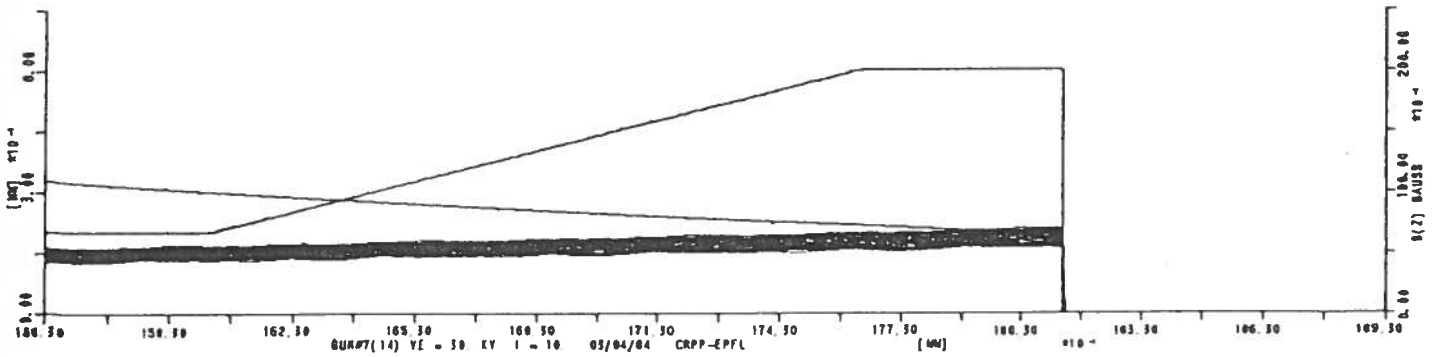
GUN#7(14) YE = 30. KY I = 10 03/04/84 CRPP-EPFL
[MM]
B(Z) GAUSS

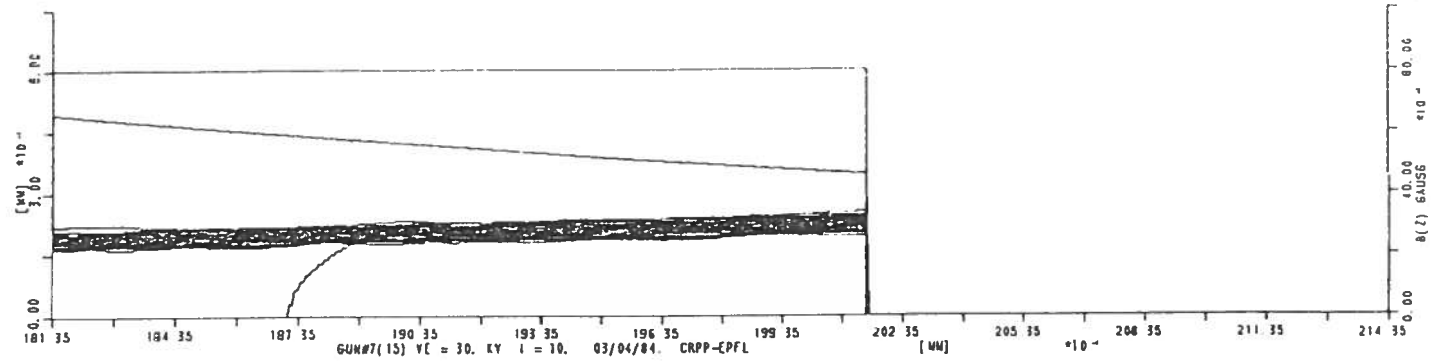
GUN#7(15) VE = 30. KV I = 10. 03/04/84. CRPP-EPFL
[MM]
B(Z) GAUSS

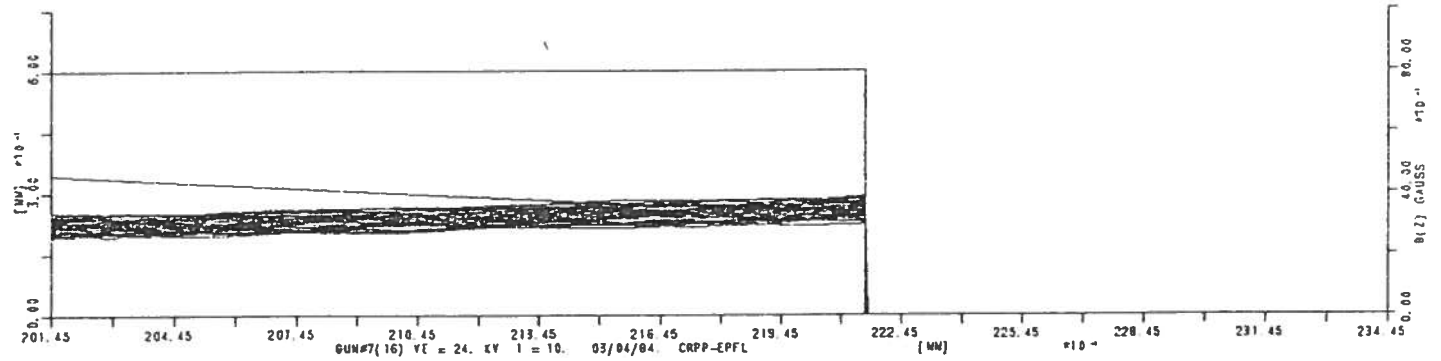
GUN#7(16) VE = 24. KV I = 10. 03/04/84. CRPP-EPFL
[MM]
B(Z) GAUSS

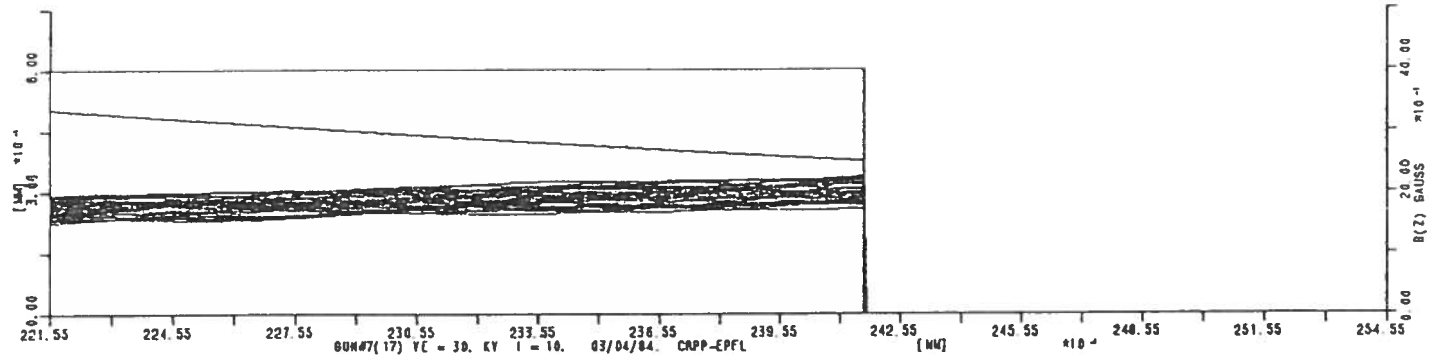
GUN#7(17) VE = 30. KV I = 10. 03/04/84. CRPP-EPFL
[MM]
B(Z) GAUSS

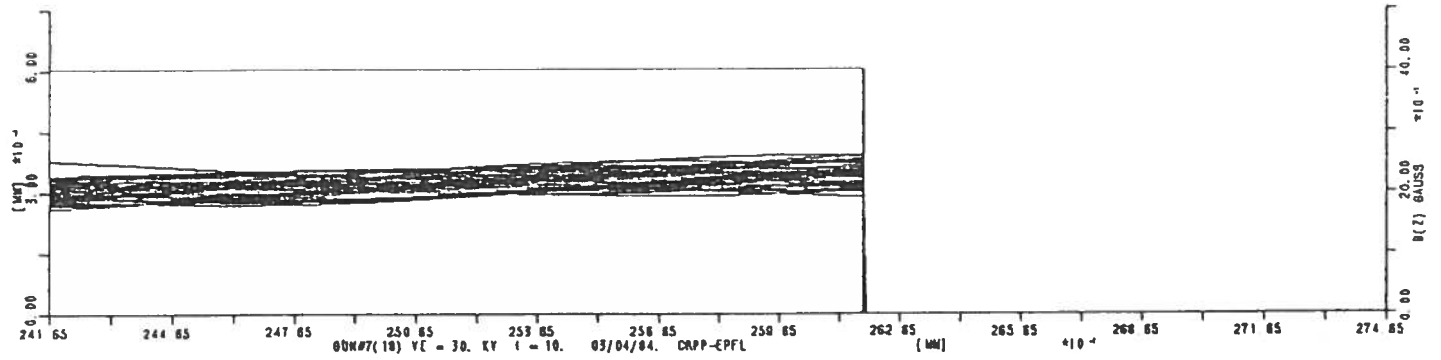
GUN#7(18) VE = 30. KV I = 10. 03/04/84. CRPP-EPFL
[MM]
B(Z) GAUSS

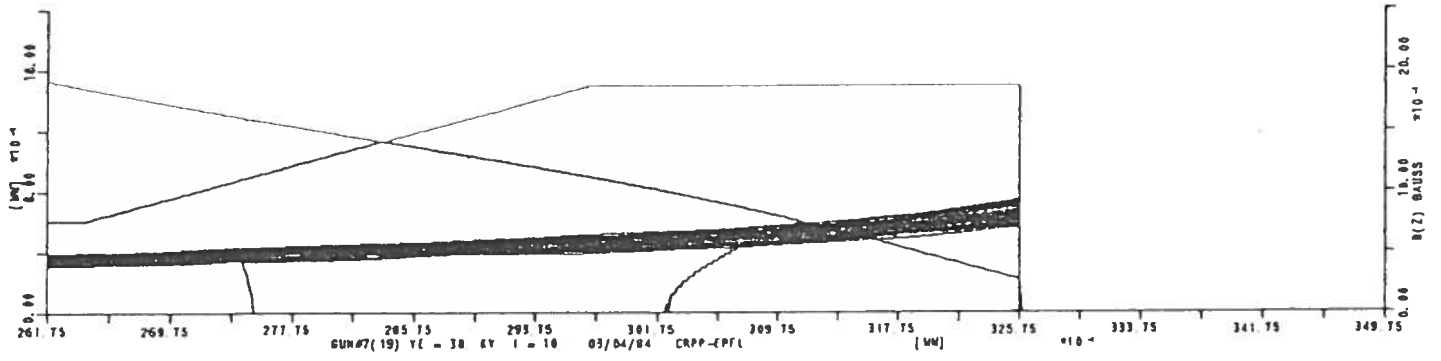
GUN#7(19) VE = 38. KV I = 10 03/04/84 CRPP-EPFL
[MM]
B(Z) GAUSS

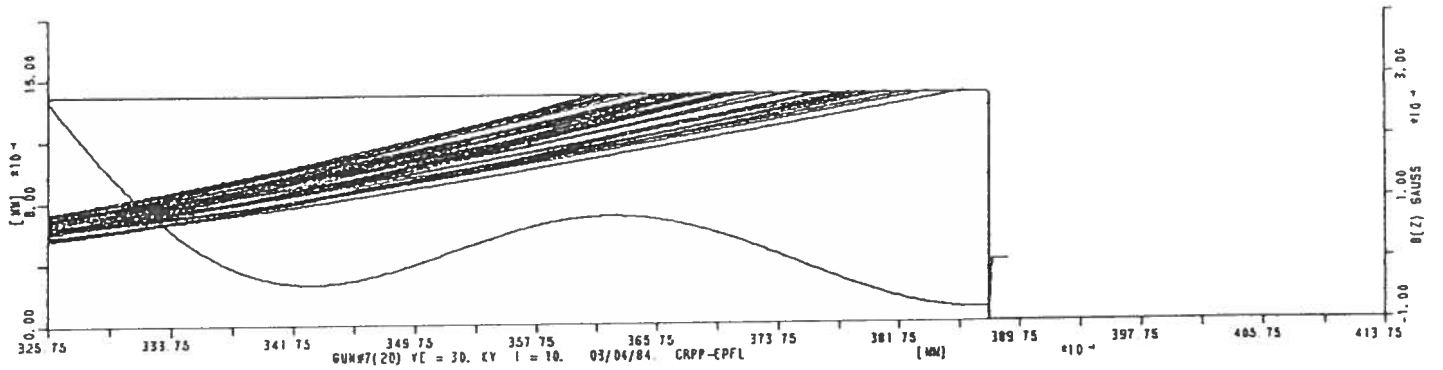
15.00
8.00
0.00
[MM] *10⁻⁴
3.00
1.00
-1.00
B(Z) GAUSS
325.75
333.75
341.75
349.75
357.75
365.75
373.75
381.75
389.75
397.75
405.75
413.75
*10⁻⁴
[MM]
GUN#7(20) YE = 30. KY I = 10. 03/04/84. CRPP-EPFL

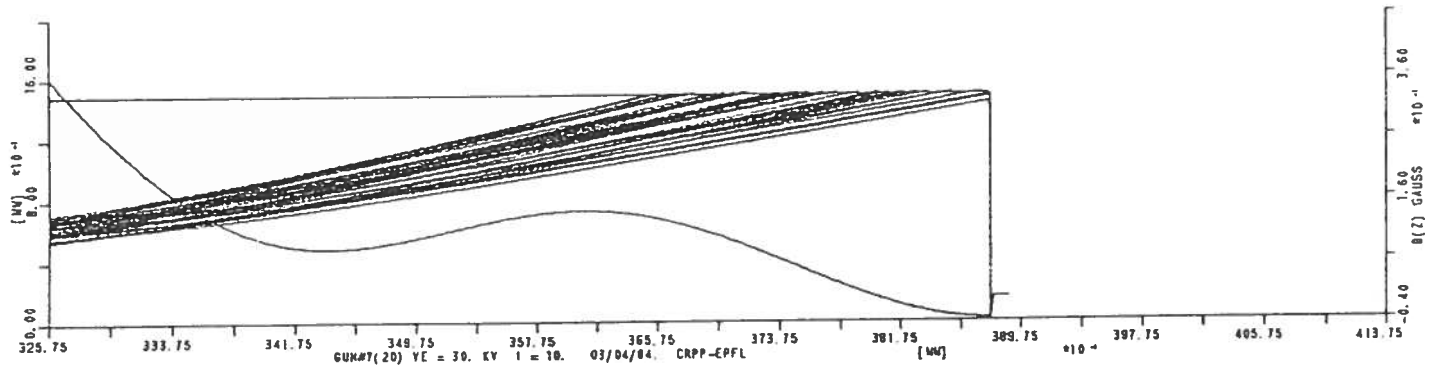
16.00
8.00
0.00
[MM] *10⁻⁴
3.60
1.60
-0.40
B(Z) GAUSS
325.75
333.75
341.75
349.75
357.75
365.75
373.75
381.75
389.75
397.75
405.75
413.75
*10⁻⁴
[MM]
GUN#7(20) YE = 30. KY I = 10. 03/04/84. CRPP-EPFL

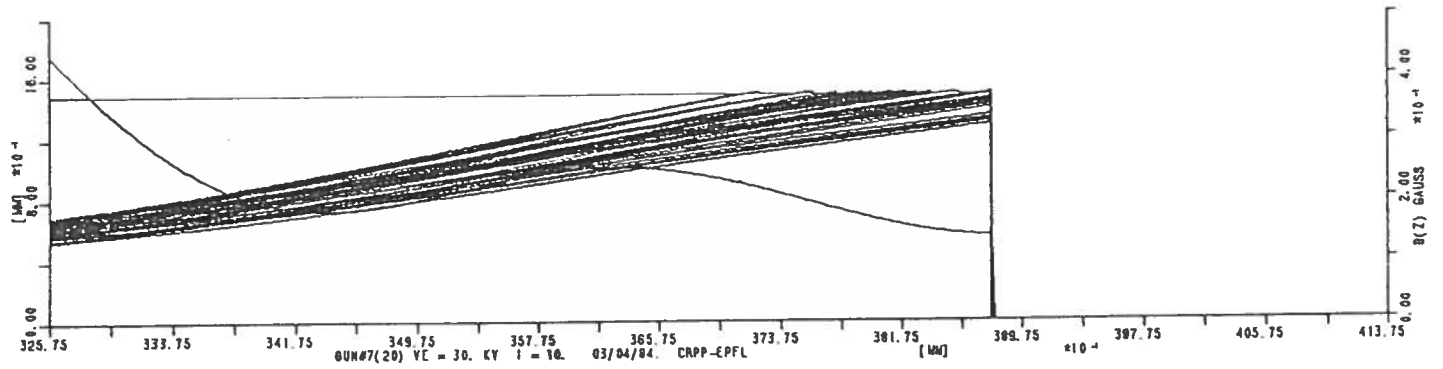
16.00
8.00
0.00
[MM] *10⁻⁴
4.00
2.00
0.00
B(Z) GAUSS
325.75
333.75
341.75
349.75
357.75
365.75
373.75
381.75
389.75
397.75
405.75
413.75
*10⁻⁴
[MM]
GUN#7(20) YE = 30. KY I = 10. 03/04/84. CRPP-EPFL

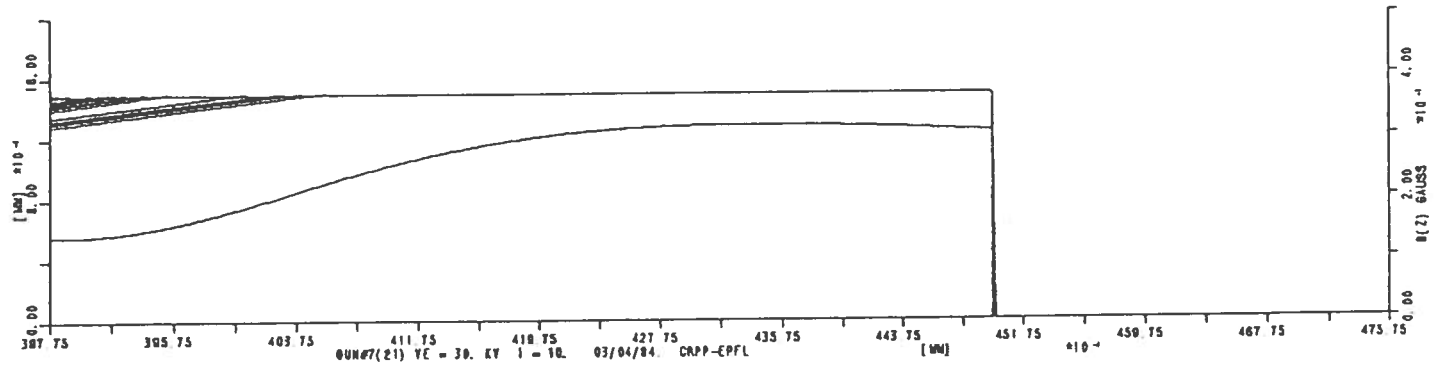
16.00
8.00
0.00
[MM] *10⁻⁴
4.00
2.00
0.00
B(Z) GAUSS
387.75
395.75
403.75
411.75
419.75
427.75
435.75
443.75
451.75
459.75
467.75
473.75
*10⁻⁴
[MM]
GUN#7(21) YE = 30. KY I = 10. 03/04/84. CRPP-EPFL

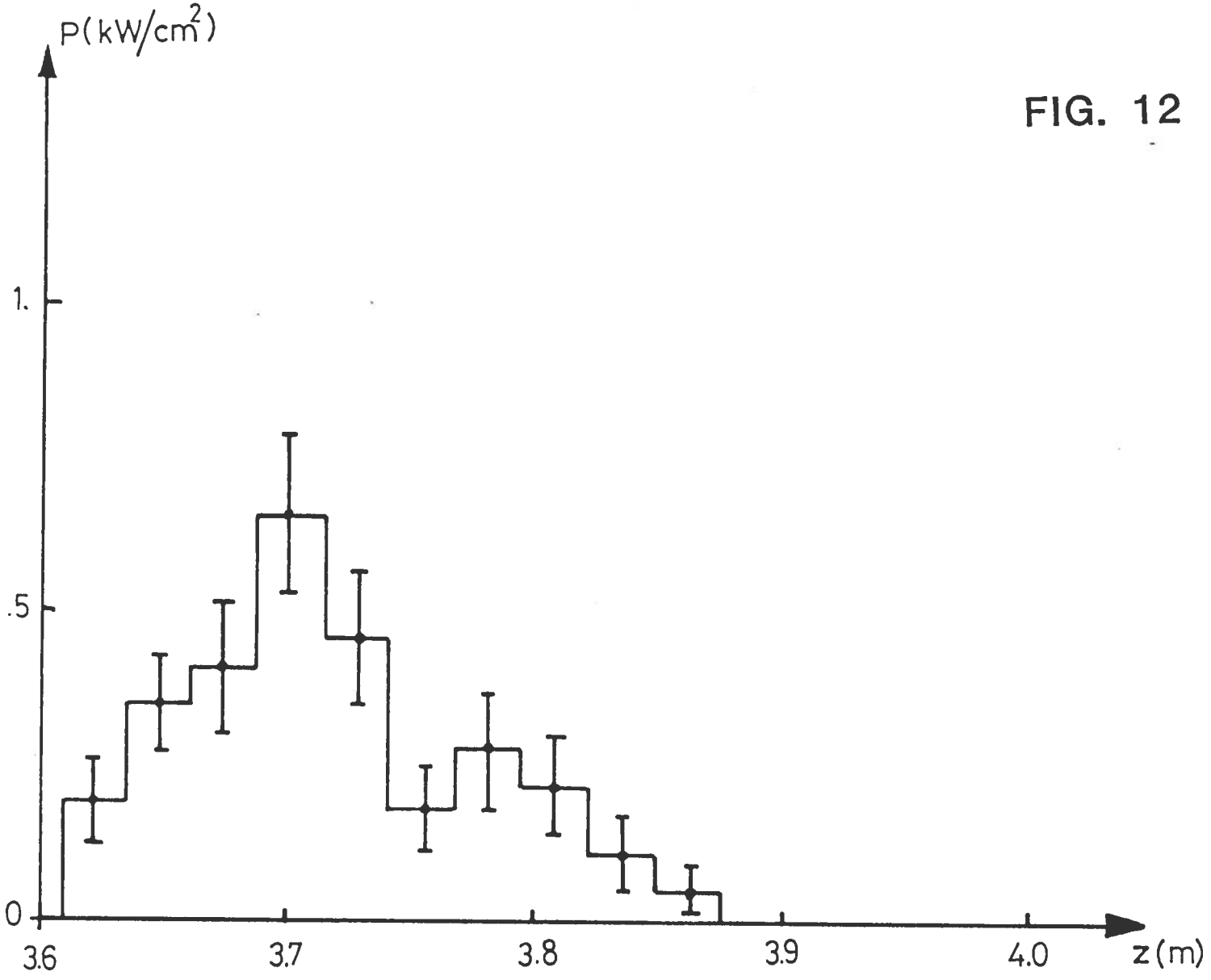

FIG. 12